NAVAL POSTGRADUATE SCHOOL

MONTEREY, CALIFORNIA

THESIS

OPTICAL AND RADIO FREQUENCY REFRACTIVITY FLUCTUATIONS FROM HIGH RESOLUTION POINT SENSORS: SEA BREEZES AND OTHER OBSERVATIONS

by

Douglass A. MacPherson

March 2007

Thesis Co-Advisors: Donald L. Walters
Kenneth L. Davidson

Approved for public release; distribution is unlimited.

THIS PAGE INTENTIONALLY LEFT BLANK

REPORT DOCUMENTATION PAGE		Form Approved OMB No. 0704-0188

1. AGENCY USE ONLY (Leave blank)	2. REPORT DATE	3. REPORT TYPE AND DATES COVERED
	March 2007	Master's Thesis

4. TITLE AND SUBTITLE Optical and Radio Frequency Refractivity Fluctuations from High Resolution Point Sensors: Sea Breezes and Other Observations	5. FUNDING NUMBERS
6. AUTHOR(S) Douglass A. MacPherson	
7. PERFORMING ORGANIZATION NAME(S) AND ADDRESS(ES) Naval Postgraduate School Monterey, CA 93943-5000	8. PERFORMING ORGANIZATION REPORT NUMBER
9. SPONSORING /MONITORING AGENCY NAME(S) AND ADDRESS(ES) N/A	10. SPONSORING/MONITORING AGENCY REPORT NUMBER

11. SUPPLEMENTARY NOTES The views expressed in this thesis are those of the author and do not reflect the official policy or position of the Department of Defense or the U.S. Government.

12a. DISTRIBUTION / AVAILABILITY STATEMENT	12b. DISTRIBUTION CODE
Approved for public release; distribution is unlimited.	

13. ABSTRACT (maximum 200 words)

High bandwidth communications and optical/RF weapons systems are being developed that are limited by atmospheric absorption and accumulated phase distortions. The need and ability to mitigate these effects depends on their magnitudes. It is difficult to numerically model the magnitudes of C_n^2 numerically and results are frequently off by an order of magnitude or more. To refine models or conduct climatologically studies for C_n^2 requires direct measurements to identify the underlying factors and provide a clear understanding of the phenomena. In situ measurements of C_n^2 are extremely sparse at RF wavelengths. This thesis utilized high speed measurements of the humidity, temperature and wind speed collected on a 10 m tower at a coastal location to simultaneously examine the optical and RF C_n^2. The humidity data were collected with a high-speed infrared humidity sensor. A three axis sonic anemometer provided wind data and a fine wire temperature sensor as well as the sonic anemometer provided temperature data. All the data were sampled at 20 Hz. This study examined a subset of 251 days of data collected at Marina, California to investigate the relative variations of optical and RF magnitudes of C_n^2 and the underlying atmospheric phenomena.

14. SUBJECT TERMS	15. NUMBER OF PAGES
C_n^2, sea breeze, high frequency data, optical turbulence	55
	16. PRICE CODE

17. SECURITY CLASSIFICATION OF REPORT	18. SECURITY CLASSIFICATION OF THIS PAGE	19. SECURITY CLASSIFICATION OF ABSTRACT	20. LIMITATION OF ABSTRACT
Unclassified	Unclassified	Unclassified	UL

NSN 7540-01-280-5500 Standard Form 298 (Rev. 2-89)
Prescribed by ANSI Std. 239-18

THIS PAGE INTENTIONALLY LEFT BLANK

Approved for public release; distribution is unlimited.

OPTICAL AND RADIO FREQUENCY REFRACTIVITY FLUCTUATIONS FROM HIGH RESOLUTION POINT SENSORS: SEA BREEZES AND OTHER OBSERVATIONS

Douglass A. MacPherson
Captain, United States Air Force
B.S., Lyndon State College, 2000

Submitted in partial fulfillment of the
requirements for the degree of

MASTER OF SCIENCE IN METEOROLOGY

from the

NAVAL POSTGRADUATE SCHOOL
March 2007

Author: Douglass A. MacPherson

Approved by: Donald L. Walters
Co-Advisor

Kenneth L. Davidson
Co-Advisor

Philip A. Durkee
Chairman, Department of Meteorology

THIS PAGE INTENTIONALLY LEFT BLANK

ABSTRACT

High bandwidth communications and optical/RF weapons systems are being developed that are limited by atmospheric absorption and accumulated phase distortions. The need and ability to mitigate these effects depends on the magnitudes of the atmospheric perturbations. The optical and RF index of refraction structure function parameters, C_n^2, are examined simultaneously using field data. It is difficult to model the magnitudes of C_n^2, accurately and values produced by models are frequently off by an order of magnitude or more. In situ measurements of C_n^2 are extremely sparse at RF wavelengths and limited to a few field studies. To refine models or conduct climatologically studies for C_n^2 requires direct measurements to identify the underlying factors that produce the fluctuations and provide a clear understanding of the phenomena. This thesis utilized high speed measurements of the atmospheric humidity, temperature and wind speed collected on a tower 10 m above ground level at a coastal location. The humidity data were collected with a high speed infrared humidity sensor. A three axis sonic anemometer provided the wind fluctuation data and a fine wire temperature sensor as well as the sonic anemometer provided atmospheric temperature. All the data were sampled at 20 Hz. This study examined a subset of 251 days of data collected at the Marina, California airport to determine the relative variations of the optical and RF magnitudes of C_n^2 and the underlying atmospheric phenomena that produced the results.

THIS PAGE INTENTIONALLY LEFT BLANK

TABLE OF CONTENTS

LIST OF FIGURES

LIST OF TABLES

THIS PAGE INTENTIONALLY LEFT BLANK

ACKNOWLEDGMENTS

First I want to thank my thesis advisors. Professor Walter's enthusiasm for this research and willingness to teach me has enriched my educational experience. Professor Davidson's insights and guidance were extremely helpful in the thesis process. Together they prepared me to go into the field and continue learning as I apply the knowledge gained at NPS.

I must also thank my children, Jessica and Alex, who have done more than they can imagine in helping me. Watching their eagerness to learn in elementary school studies has been an inspiration for my own studies.

I'm indebted to Richard Lind for the education on the art and technicalities of making precise meteorological measurements.

I would also like to express my appreciation to Professor Wang and the Office of Naval Research who are responsible for the Marina flux tower instrumentation as part of the NPS/NRL CBLAST project.

THIS PAGE INTENTIONALLY LEFT BLANK

I. INTRODUCTION

A. OBJECTIVES

Understanding the refractive index structure function parameter (C_n^2) and related parameters is essential when dealing with optical and radio propagation. A wide array of techniques for measurement of optical turbulence have been developed (Eaton 2005). High-speed point measurements of the temperature and humidity fluctuations provide a direct means to determine the optical (dry) and RF (wet) C_n^2 simultaneously.

The Naval Postgraduate School (NPS) Department of Meteorology, Monterey, CA, operates a sensor suite designed for flux measurements near the airport in Marina, CA. This suite includes a three-axis sonic anemometer, a fine-wire temperature probe and a humidity measuring system all taking measurements at a frequency of 20 Hz. The data collected from these sensors was used to measure C_n^2 and the related parameters directly.

An important phenomena characterizing this and similar coastal overland locations is the land-breeze - sea-breeze wind reversal that occurs frequently, almost every day. Airflow data measured with the Marina site flux measurement suite from October 2005 to June 2006 were used to investigate how the optical and RF C_n^2 depends on the atmospheric wind flow and solar heating patterns. Furthermore, distinct sea breeze frontal passages were examined in detail to understand the abrupt changes in temperature and humidity that occur during these transitions.

B. BACKGROUND

1. Index of Refraction

The atmospheric index of refraction depends on pressure, temperature and humidity. The relative contribution of these variables changes with wavelength. For visible and near-infrared radiation, temperature fluctuations dominate the process. It is customary to use a reference wavelength value of 0.5 μm and the resulting equation for index of refraction is:

$$n - 1 = 79 \times 10^{-6} \frac{p}{T} \quad , \tag{1}$$

where n is the index of refraction, T is the temperature in degrees Kelvin, p is the pressure in mb (Beland 1996). Assuming that atmospheric turbulence occurs at speeds much less than the speed of sound, the change in the index of refraction n for an isobaric change in temperature is

$$dn = \left(-\frac{79}{T^2} p \, dt \right) \times 10^{-6} \tag{2}$$

At millimeter and centimeter wavelengths the effects of water vapor molecular rotations are substantial. Tatarski (1961) provided the following expression for the real part of the index of refraction that is valid for radio waves of centimeter wavelength:

$$n - 1 = 10^{-6} \times \frac{79}{T} \left(p + \frac{4800e}{T} \right) \tag{3}$$

where n is the index of refraction, T is the temperature in degrees Kelvin, p is the pressure in mb and e is the water vapor pressure in mb. The corresponding change in index of refraction for changes in both temperature and the water vapor partial pressure is

$$dn = \left[-\left(\frac{79}{T^2} p + 2 * \frac{379200}{T^3} e \right) dt + \frac{379200}{T^2} de \right] \times 10^{-6} \quad (4)$$

At RF wavelengths the humidity term often dominates the temperature term and the total change in *n* will depend on whether the changes in humidity and temperature add or subtract.

2. Kolmogorov Turbulence Variance Statistics

For many geophysics processes, the conventional variance is not a robust statistic because the mean value is not stationary. Kolmogorov introduced a more advanced statistic based on structure functions. By assuming homogeneity and isotropy at least in a local volume, and if the random processes vary slowly, structure functions represent the mean square difference in the fluctuations of $f(r_1,r_2)$ over a distance r_1 and r_2 between the two measurements (Tatarski 1961).

$$D_f(r_1, r_2) = \left\langle \left[f(r_1) - f(r_2) \right]^2 \right\rangle \quad (5)$$

Structure functions avoid the nonstationary mean issue and provide robust statistical descriptions of turbulent phenomena. Although the wind velocity is the dominant physical process involved in turbulence, the wind can carry passive additives like temperature and humidity with the turbulent flow. The passive additives pick up the same statistical characteristics from the turbulent flow and share similar statistical characteristics (Tatarski 1961).

According to Kolmogorov turbulence theory, turbulent eddies range in size from macro-scale to micro-scale forming a continuum of decreasing eddy sizes. Energy from convection and wind shear is added to the system at the outer scale L_0 (10's - 100's of meters) before it cascades to a smaller scale l_0 (1cm or less) where viscosity converts the energy to heat, Fig. 1 (Max 2006).

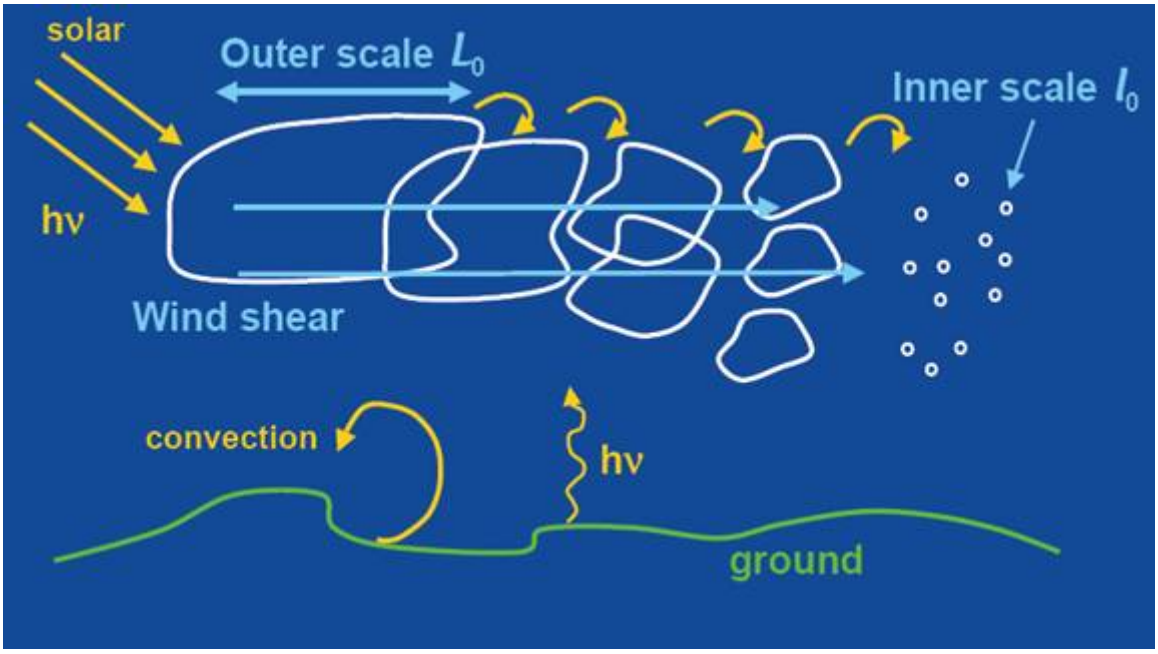

Figure 1. Illustration of Kolmogorov turbulent eddies cascading down in the inertial dissipation range between the outer scale and the inner scale. (Max 2006)

With dimensional arguments and assuming a homogeneous incompressible isotropic, medium, Kolmogorov showed that the longitudinal structure function of the velocity is:

$$D_v(r) = C_v^2 r^{2/3}, \qquad l_0 < r < L_0. \tag{6}$$

C_v^2 is the structure function parameter that applies to the property specified by γ, and $r = |r_2 - r_1|$ is the spatial separation between the two measurements. The $r^{2/3}$ proportionality of the structure function in the inertial range ($l_0 < r < L_0$) also applies to the passive additive structure functions such as those for temperature, for humidity, and for refractive index (Tatarski 1961)

3. Optical Turbulence

Optical turbulence is the result of temporal and spatial fluctuations of the index of refraction resulting from atmospheric turbulence. In a basic differential form C_n^2 is a function of three elements and by squaring Eq. (4) is

$$\mathrm{C}_{\mathrm{n}}^2 = \left(\frac{\partial n}{\partial T}\right)^2 \mathrm{C}_T^2 + \left(\frac{\partial n}{\partial q}\right)^2 \mathrm{C}_q^2 + 2\left(\frac{\partial n}{\partial T}\right)\left(\frac{\partial n}{\partial q}\right)\mathrm{C}_{qT} \tag{7}$$

where C_T^2 represents the temperature structure parameter, C_q^2 represents the structure parameter for humidity, and C_{qT} cross covariance between temperature and humidity. Eq. (7) is often written in terms of the potential temperature or virtual potential temperature particularly when considering variations over altitude such as with radar data (Stankov 2003). At optical frequencies, humidity generally has a negligible contribution except over saturated soil and maritime surfaces where its contribution to total C_n^2 can reach 20%, mainly through the C_{qT} term (Beland 1996).

For Kolmogorov turbulence the refractive turbulence structure function parameter C_n^2 is

$$C_n^2 = \left\langle (n_1 - n_2)^2 \right\rangle \Big/ r^{2/3}, \tag{8}$$

which is the mean-square statistical average of the difference in the indices of refraction, $n_1 \, and \, n_2$, between two points (Parker 2002). The angle brackets represent the ensemble average and r is the distance between the two points. Differences in the index of refraction are caused by localized changes in temperature and humidity resulting from turbulent mixing of the atmosphere. A typical value of r used to determine C_n^2 is one meter.

C_T^2 is computed in the same manner yielding:

$$C_T^2 = \left\langle (T_1 - T_2)^2 \right\rangle \Big/ r^{2/3} \tag{9}$$

By taking the partial derivative of the Eq. (1) with respect to the temperature and assuming the turbulent eddies are isobaric C_n^2 is related to the temperature structure function (C_T^2) with the following equation:

$$C_n^2 = (79 \times 10^{-6} P / T^2)^2 C_T^2 \ , \tag{10}$$

where P is the atmospheric pressure in millibars and T is the temperature in Kelvin (Tatarski 1961).

With high resolution temperature and humidity data measured simultaneously Eqs. (1) and (3) provide a means to compute C_n^2 directly from

$$C_n^2 = \left\langle (n_1 - n_2)^2 \right\rangle \Big/ r^{2/3} , \tag{11}$$

This technique allows a direct comparison of the optical (dry) and RF (moist) C_n^2 variations throughout a day as the underlying turbulent, atmospheric processes evolve by choosing the appropriate dry and moist expressions for n, Eqs (1) and (3) respectively. Part II of this thesis will introduce a more recent and refined version of the RF refractivity equation that was used for the data reduction.

C. MEASUREMENT CHALLENGES

1. Taylor's Hypothesis

Turbulence affects optical propagation through temporal and spatial distortion of the wave-front. Taylor's hypothesis is an approximation that allows for estimating spatial turbulence statistics using measurements from air moving past a single point. For low intensity turbulence in a uniform mean flow the turbulence pattern is assumed to be "frozen". This hypothesis is valid under most conditions, but becomes questionable when free convection velocity fluctuations are of the same order or larger than the mean velocity, or when the frequency of the turbulent eddies is not significantly higher than the magnitudes of the mean wind shear (Arya 2001).

2. Nyquist Frequency

The data sample rate f_s determines highest frequencies that are resolved in a continuous time series. The Nyquist frequency f_n is the highest frequency resolved in the sampled data set. To prevent aliasing a wave must be sample at least twice per period so the Nyquist frequency is $f_n = \frac{f_s}{2}$.

3. Sampling Requirements

Combining Taylor's hypothesis guidance and the Nyquist frequency constraints poses a significant challenge when trying to measure turbulent eddies that range in size from centimeters up to meters with measurement at a single point. As the mean wind speed increases the required sampling frequency increases. Likewise, as the eddy sizes decrease the sampling frequency must increase.

Satisfactorily resolving features in the centimeter range with typical mean flows of several meters per second requires instrument response times in milliseconds. Typically fine wire temperature probes, high frequency sonic systems, radars and lasers are used to measure such features at the necessary frequency.

Table 1 shows the required sample frequency based on eddy wavelength and mean wind speed. The data used for this thesis was sampled at 20 Hz so frequencies in the highlighted areas represent what can be resolved from the data.

Required Sample Frequency (Hz)							
Mean flow	Eddy wavelength (m)						
U(m/s)	0.01	0.05	0.1	0.25	0.5	1	2
0.5	100	20	10	4	2	1	0.5
1	200	40	20	8	4	2	1
1.5	300	60	30	12	6	3	1.5
2	400	80	40	16	8	4	2
2.5	500	100	50	20	10	5	2.5
3	600	120	60	24	12	6	3
3.5	700	140	70	28	14	7	3.5
4	800	160	80	32	16	8	4
4.5	900	180	90	36	18	9	4.5
5	1000	200	100	40	20	10	5
5.5	1100	220	110	44	22	11	5.5
6	1200	240	120	48	24	12	6
6.5	1300	260	130	52	26	13	6.5
7	1400	280	140	56	28	14	7
7.5	1500	300	150	60	30	15	7.5
8	1600	320	160	64	32	16	8
8.5	1700	340	170	68	34	17	8.5
9	1800	360	180	72	36	18	9
9.5	1900	380	190	76	38	19	9.5
10	2000	400	200	80	40	20	10

Table 1. Required sample rates as a function of mean wind and feature size.

D. MARINA FIELD SITE SENSORS

1. Location

The NPS Marina Field Site sensor site is located 1.5 km north-north east of the runway at the Marina airport (formerly Fritzsche Army airfield). The sensor is approximately 4.7 km east of Monterey Bay and 40 meters west of a small bluff overlooking the Salinas valley, Fig. 2. The site is approximately 51 m above mean sea level and includes a 10 m tower for the flux measurements sensor suite.

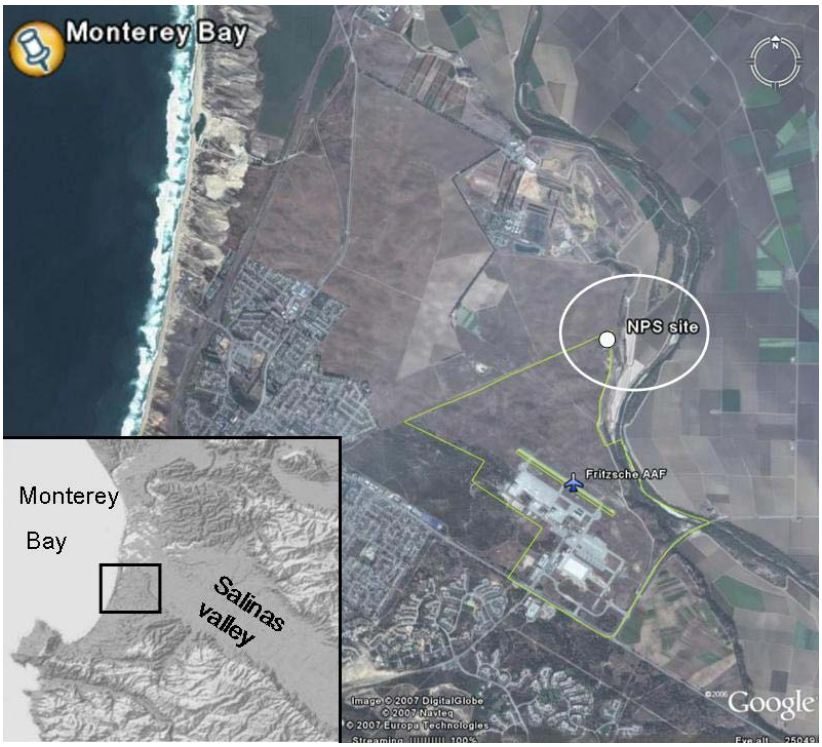

Figure 2. Location of NPS sensor site in Marina CA.

Wind at the site is primarily driven by two factors: Land and sea breezes, which have due east or westerly winds (Fort Ord TRFN 1977) and the orientation of the Salinas Valley, which produces north-east and south-west winds. The three sensors that collected the data for the C_n^2 calculations were mounted about 9.5 meters above the surface facing a direction of 210°. This allows for the for minimal flow disturbance from the tower and support apparatus during the most common wind flows, Fig. 3.

Figure 3. 3-axis sonic anemometer with a fine wire temperature probe extending from the left side of the mount and the open path gas analyzer mounted to the right. (picture by Richard Lind of NPS)

2. Sensors

a. Ultra-Sonic Anemometer

Sensors for examining C_n^2 have to sample the influencing airflow properties fast enough to describe the relevant turbulent intensity and correlation. The sensors installed at the Marina Field site included a three-axis sonic anemometer, a CSAT3 manufactured by Campbell Scientific Inc. It uses three pairs of non-orthogonally oriented ultrasonic transducers. Horizontal wind velocity and direction along with vertical velocities are derived from the measured time of flight for the ultrasonic signals (manufacture's instruction manual).

The anemometer is capable of sampling at frequencies from 1 to 60 Hz. During the measurements for the period studied, the anemometer sampled at 60 Hz and the data were block-averaged to achieve 20 Hz output data. Because the speed of sound is primarily dependant on temperature, the CSAT3 measurements also provided estimates of air temperature from the path-average speed of sound along the three sensor paths. This derived temperature

is density-based and referred to as the sonic virtual temperature (T_s), dependent of water vapor as well as temperature. The CSAT3 computes the sonic temperature, T_s, in degrees Celsius, without this correction, with the following formula:

$$T_s = \frac{c^2}{\gamma_d R_d} - 273.15 \quad (12)$$

where c is the speed of sound, γ_d is the ratio of specific heat of dry air at constant pressure to that at constant volume (1.4), and R_d is the gas constant for dry air ($287.04\ JK^{-1}\ kg^{-1}$).

b. Fine Wire Thermocouple

The sonic anemometer has limitations with regard to evaluating optical turbulence from the influence of humidity on temperature estimations and from the measurement being a path average. This introduces a temperature uncertainty and a low-pass filter effect on the temperature turbulence statistics. A high response fine wire thermocouple, a Campbell Scientific FW1 collocated with the CSAT3 at the Marina Field site, also provided temperature fluctuations. The FW1 uses a 0.0254 mm wire. The fine wire's small diameter allows millisecond response times and measurement at 20 Hz (Roper 1992). The small diameter also minimizes solar loading to the point where a shelter is not needed for the sensor (manufacture's brochure), although the fine wire is susceptible to breakage.

c. Open Path Gas Analyzer

Because humidity fluctuations influence C_n^2 and are a critical component of the RF atmospheric index of refraction, a high-speed sensor for humidity was important. The LI-7500 manufactured by Licor is an open path gas analyzer designed to measure H_2O and CO_2 in the air. It transmits an infrared

beam and measures attenuation as 4 wavelengths; attenuation at non-absorbing wavelengths ($3.95\,\mu\mathrm{m}$ and $2.40\,\mu\mathrm{m}$) is measured as a reference. Then absorption centered at $4.26\,\mu\mathrm{m}$ $2.59\,\mu\mathrm{m}$ is measured to determine CO_2 and water vapor respectively (manufacture's description). Measurements can be made a 5, 10, or 20 Hz, data collected for this project was 20 Hz.

The LI-7500 also has a barometer housed in a junction box attached to the tower. This provides the pressure data used in this project. This sensor does not sample at high frequency. The scale of turbulence studied, the inertial subrange, is isobaric in nature so the high frequency pressure data is not required.

II. DATA AND ANALYSIS

A. INTRODUCTION

Understanding phenomena being examined and the capabilities and limits of sensors providing data requires a strategy for analyzing the data. Several hypotheses and assumptions are applied in the strategies. For example, using Taylor's Hypothesis allows C_n^2 to be extracted by direct application of the structure function without using the more complex formulae needing power density spectra obtained from time series of varying signals.

B. TURBULENCE EXTRACTION STRATEGY

1. Application Taylor's Hypothesis

The first requirement for analyses of the fixed point measurement is an estimate of the size of the turbulent eddies causing the fixed point measured fluctuations. For the purposes of this study size a separation distance of 1.0 m was used for most of the data reduction. With a 20 Hz sample rate the number of sample points that make up a one meter segment is

$$\mathrm{SP} = \frac{f}{\overline{\mathrm{U}}} \tag{13}$$

where SP is the number of sample points required, f is the sampling frequency, and $\overline{\mathrm{U}}$ is the mean horizontal wind velocity.

To determine $\overline{\mathrm{U}}$, a second order Butterworth filter was used with a cut of frequency of 0.001 of the Nyquist frequency. The low bypass Butterworth was used instead of simple averaging to limit the impact of extreme outliers and erroneous data. The $\overline{\mathrm{U}}$ values obtained from this method are approximately equal to a one minute running average.

2. Computing Refractivity (N)

a. Radio Frequency

For this work, Rueger provides an expression for the refractivity N that is more accurate than Eq. (3) (Rueger 2002):

$$N = (n\text{-}1)\times 10^6 = \frac{77.689\times P_d}{T} + \frac{71.2925\times e}{T} + \frac{375463\times e}{T^2}, \quad (14)$$

where P_d is the partial pressure of dry air in millibars, T is the temperature in degrees Kelvin, and e is the partial air pressure of water vapor. This expression incorporates the current atmospheric CO_2 increases.

b. Optical Wavelengths

For optical wavelengths we simply use the dry component of Rueger's radio frequency formula,

$$N = \frac{77.689\times P_d}{T}, \quad (15)$$

where P_d is the partial pressure of dry air in millibars, T is the temperature in degrees Kelvin.

3. Computing C_n^2

a. Data and Point Selection

C_n^2 derived from Eq. (8) requires a length within the inertial subrange, 1 m for this research, and values of refractivity from the two points at ends of that length. The main challenge is determining how many sample points make up that 1 m length. A secondary challenge is determining which temperature values to use. After these are done satisfactorily it is simply a

process of then applying the resulting data to the structure function parameter calculation, Eq. (8).

b. Sonic Versus Fine Wire Temperatures

A decision was made to use the sonic virtual temperatures values, obtained from the CSAT3, based on the discovered effects of solar radiation on the fine wire thermocouple. During hours of darkness and light winds the fine wire and sonic temperatures are nearly equal as would be expected based on theory the pressure temperature and humidity levels on the days examined. However after sunrise a noticeable difference arises between the two values, Fig. 4. In addition to the time of day associated with the difference, the conclusion that the difference is solar induced is further supported by the fact the difference nearly disappears after the sea breeze front passes and wind speeds increase. The stronger wind speed ventilates the fine wire sensors sufficiently and minimized the solar heating effect.

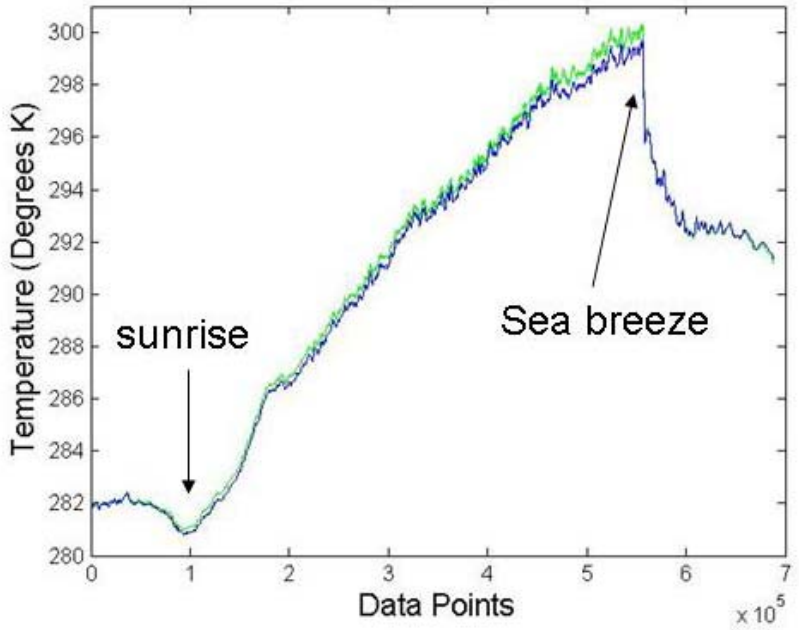

Figure 4. Fine wire T (green) and sonic T (blue) for 1400-2300 UTC 17 November 2005

The structure function parameter that defines C_n^2 is based on the spatial differences of passive variables. The spatial offset between the fine wire thermocouple and the measurement axes of the sonic anemometer was one factor in the decision not to use the fine wire data for C_n^2 determination. In addition, probe breakage reduced the available data to process. However the fine wire data provided a good way to verify the performance of the CAST3. The sonic temperature (CAST3) is derived from same sonic measurement used for wind velocity used for application of Taylor's hypothesis, so problems with spatial and temporal offset do not arise. The issues with the sonic temperature, as discussed, are the influence of humidity fluctuations on the basic measurement and low-pass filter effect due to the path average. It should also be noted that the sonic derived temperature is altered by changes in the absolute humidity. However this difference is negligible in this situation. Fig. 5 illustrates the variations in temperature and humidity differences.

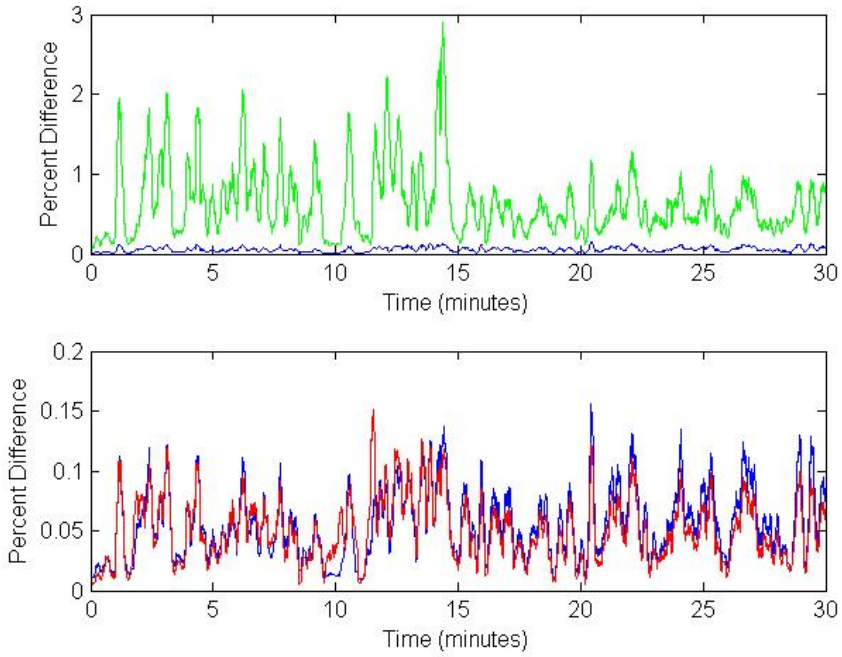

Figure 5. Top: The percent change in the humidity (green) compared to the change in sonic T (blue)
Bottom: The percent change in the fine wire T (red) compared to the change in sonic T (blue) for 2100-2130 UTC 23 February 2006

C. VERIFICATION OF C_n^2 DETERMINATION STRATEGY

1. Values

The initial verification of the chosen C_n^2 extraction strategy was to check if the resulting C_n^2 values are within the range of values measured by other methods (10^{-14} to 10^{-11} $m^{-2/3}$). The results are consistent with expected values, as shown in the Fig. 6 example set (Walters 1991).

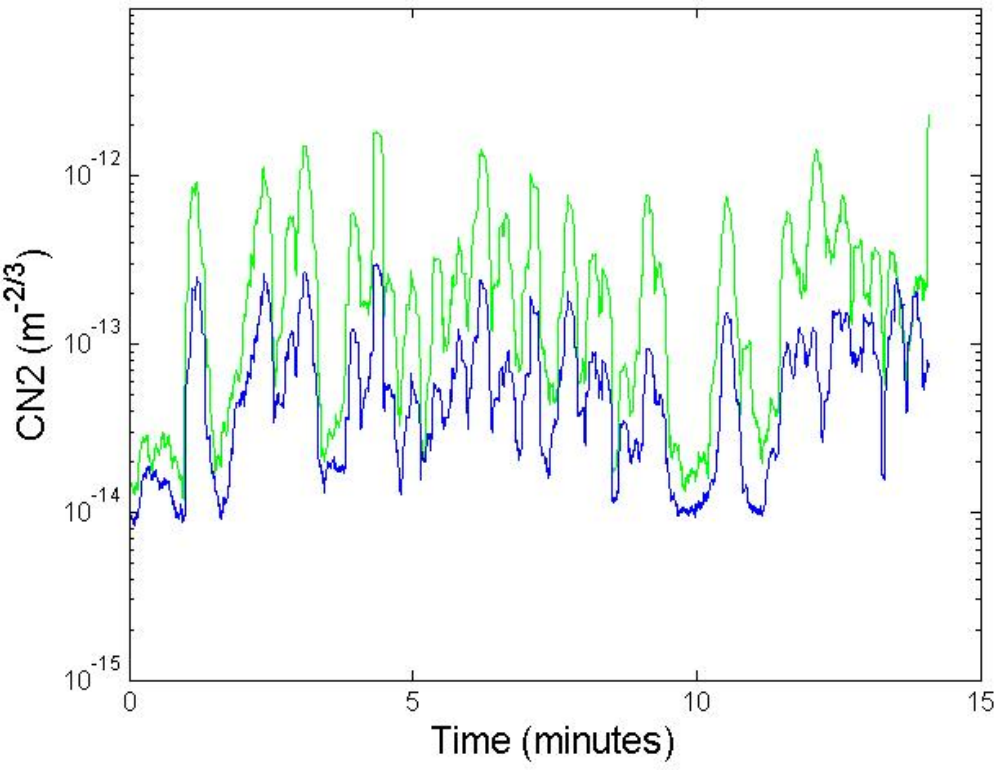

Figure 6. Wet (green) and dry (blue) C_n^2 values derived directly from the structure function, 2100-2115 UTC on 23 February 2006

2. Power Spectral Density

The values of C_n^2 are determined by passive variables (temperature and humidity) being mixed by turbulent flow. In the inertial sub range this turbulence follows the Kolmogorov theory. Therefore the log plot of power spectral density

for passive variables, or the quantities such as refractivity (N) determined by these variables, should show a $f^{-5/3}$ dependence in the frequency domain. This was seen consistently as the example in Fig. 7 illustrates.

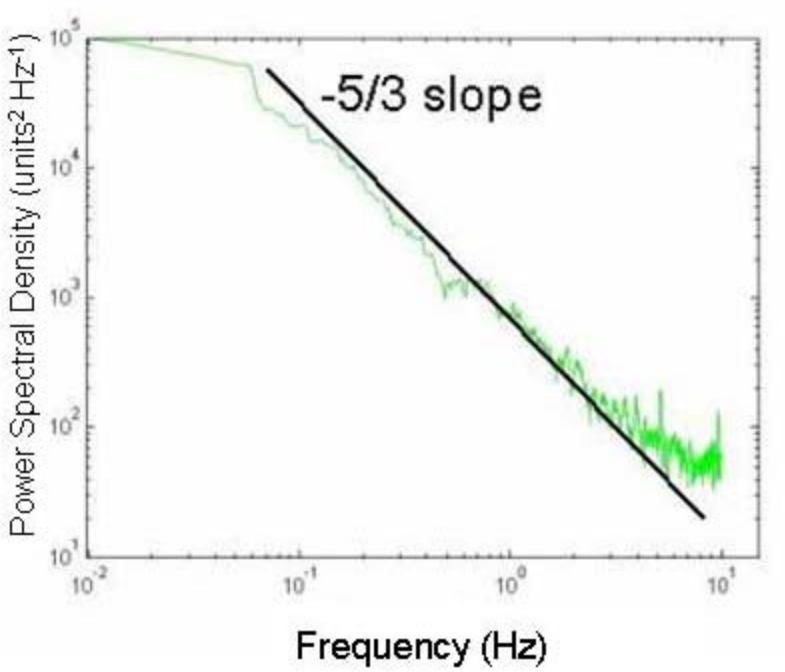

Figure 7. Power spectral density of C_n^2 generate from 4096 data points (~3.5 min of data) beginning at 2147 UTC 17 November 05

During the time period corresponding to Fig. 7 the mean wind velocity was approximately 4 m s^{-1} for which, with the structure function distance set a 1 m, the resulting Nyquist frequency is 8 Hz. The departure from a $f^{-5/3}$ slope at high frequencies, above 2 Hz, should not be interpreted as a departure from Kolmogorov theory. It is likely the result of noise in the signal as the sensor limitation (Nyquist frequency) is approached. The height of the data collection from the ground (9.8m) also imposes an outer scale at low frequencies.

D. TEMPERATURE AND HUMIDITY CORRELATION

1. Radio Frequency and Optical C_n^2 Differences

There were times when the RF C_n^2 was larger than the optical C_n^2 case. These events occurred with a negative correlation between temperature and humidity. Figures 8 and 9 provide a clearer illustration of these phenomena around the 45 minute point. When the optical C_n^2 is higher than the RF case the temperature and humidity correlation is positive.

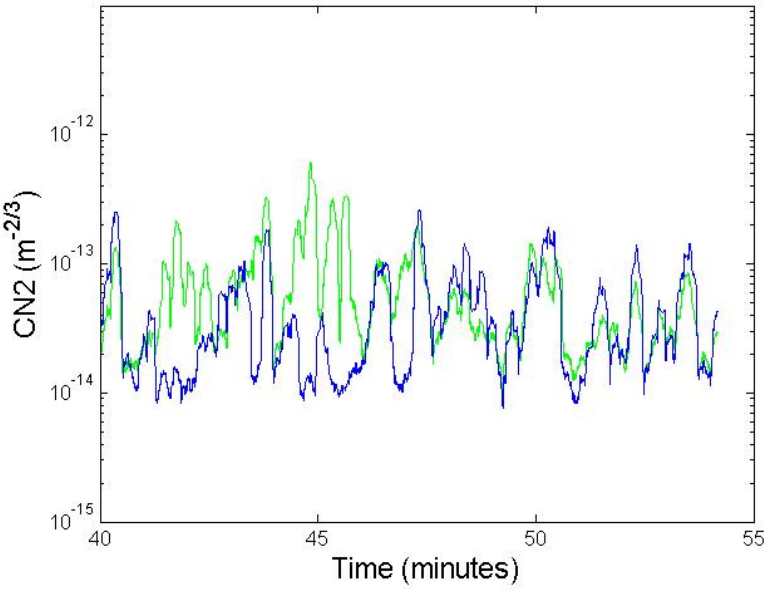

Figure 8. RF C_n^2 (green) and optical C_n^2 (red) from 2140-2155 UTC on 6 December 2005

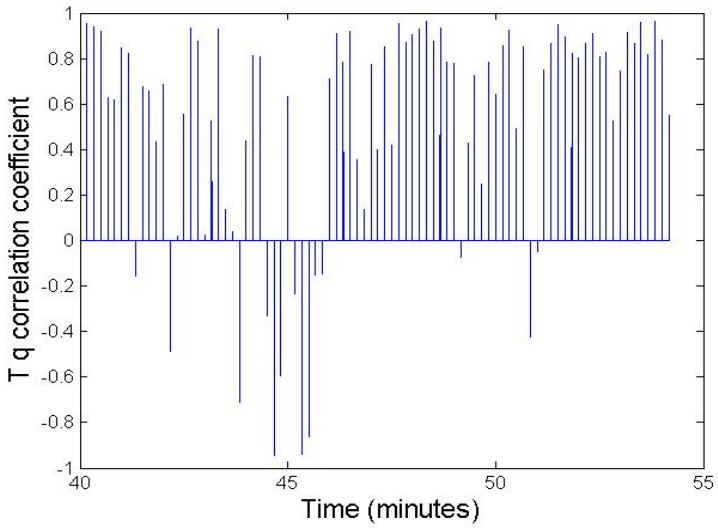

Figure 9. Temperature and humidity correlation coefficient from 2140-2155 UTC on 6 December 2005

To further investigate the phenomena of the RF C_n^2 versus optical C_n^2 difference, the refractivity N_2-N_1 in the moist and dry components of N 1 m apart were plotted. The last two terms of Eq. (14) are the moist component of N. The first term of Eq. (14) is the dry term (and also the only term in Eq. (15) for optical N). The difference of these components over one meter is plotted in Fig 10.

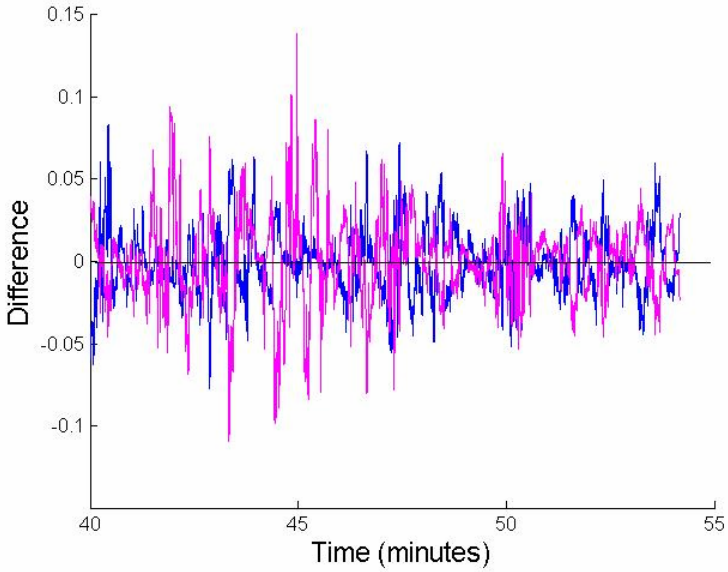

Figure 10. Refractivity difference N_2 –$N_1$of the separate dry N (blue) and moist N contributions to the refractivity (magenta) from 2140-2155 UTC on 6 December 2005

2. Phase and Magnitude

Fig. 8 and 9 show that when the optical C_n^2 exceeds the RF C_n^2 the moist and dry components of N are out of phase. This can only occur when temperature and humidity are positively correlated. The magnitude of the change humidity term in Eq. (14) is great enough to dominate the effects of the change in temperature and cause the moist and dry components of N to cancel.

The temperature and humidity values between the 44 and 46 minute points are primarily negatively correlated (Figure 9), or the humidity fluctuations overwhelm the temperature changes. The influence of the humidity and temperature terms in Eq. (14) explains the large increase in the RF C_n^2 during these times.

THIS PAGE INTENTIONALLY LEFT BLANK

III. CASE STUDIES

A. DAY SELECTION

The available multi-sensor data set spanned 251 days. Numerous days had missing or unreliable data for different sensors required to determine C_n^2 . These missing or unreliable data were caused by broken fine wires or contaminated lenses on the LI-7500. Within the set of days with all sensors operating, there were six that had clear skies and distinct sea breeze fronts. From these, two days (17 November 2005, and 23 February 2006) with what were interpreted to be the most well-defined see breeze fronts were selected for detailed analyses and interpretation of C_n^2 variations and impacting factors.

Neither of the previously mentioned days had a complete 24 hours of data. To view a diurnal cycle, a day with 24 hours of good data was analyzed (26 November 05).

B. 17 NOVEMBER 2005

1. General Conditions

The meteorological conditions on 17 November 2005 were nearly perfect for examining a sea breeze front Fig. 11. There were weak synoptic forcing conditions with offshore winds less than 4 m s^{-1}. Clear skies as indicated by the shortwave irradiance curve permitted strong solar heating as indicated on the temperature plot. At approximately 2145 UTC (1345 PST) the passage of the sea breeze front was clearly marked by a rapid change in wind direction from offshore (~080^o) to onshore at the field site location (~270^o) and by wind speed increasing (from less than 2 m s^{-1} to above 4 m s^{-1}), and with increasing dew points and decreasing temperatures. Increases in the wind speed forced corresponding changes in C_n^2 by causing increases in mixing of airflow

temperature and humidity resulting in lower vertical gradients in the overlying airflow.

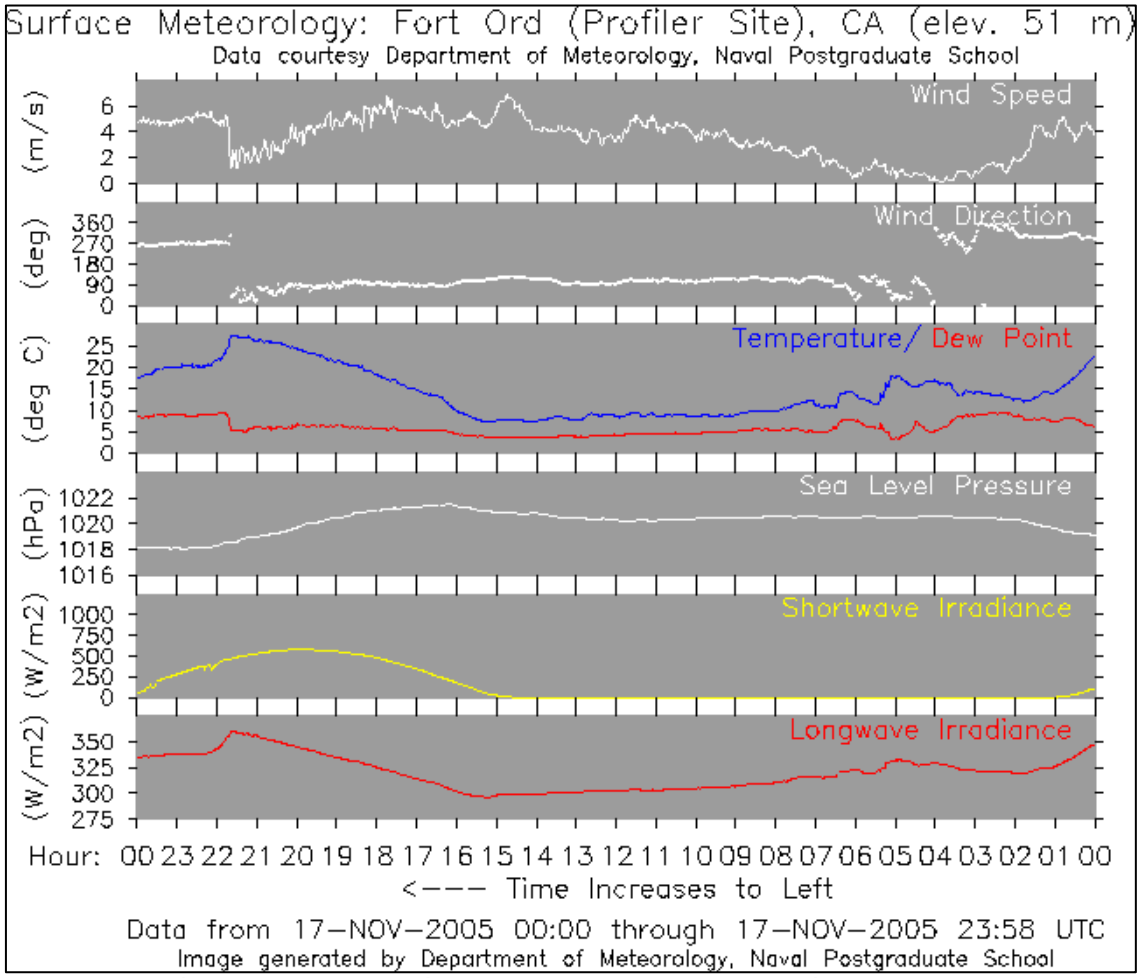

Figure 11. Weather summary for 17 November 2005

2. Sea Breeze Shift

Examination of the 30-minute block containing the sea breeze the data from the CSAT-3 and the LI-7500 also shows the very distinct sea breeze as seen in Fig. 12. Over a period of approximately 30 seconds there is a temperature decrease (~ 4°K), an absolute humidity increase (~ 2 g m^{-3}), and a doubling of the wind velocity from ~2 m s^{-1} to ~4 m s^{-1}.

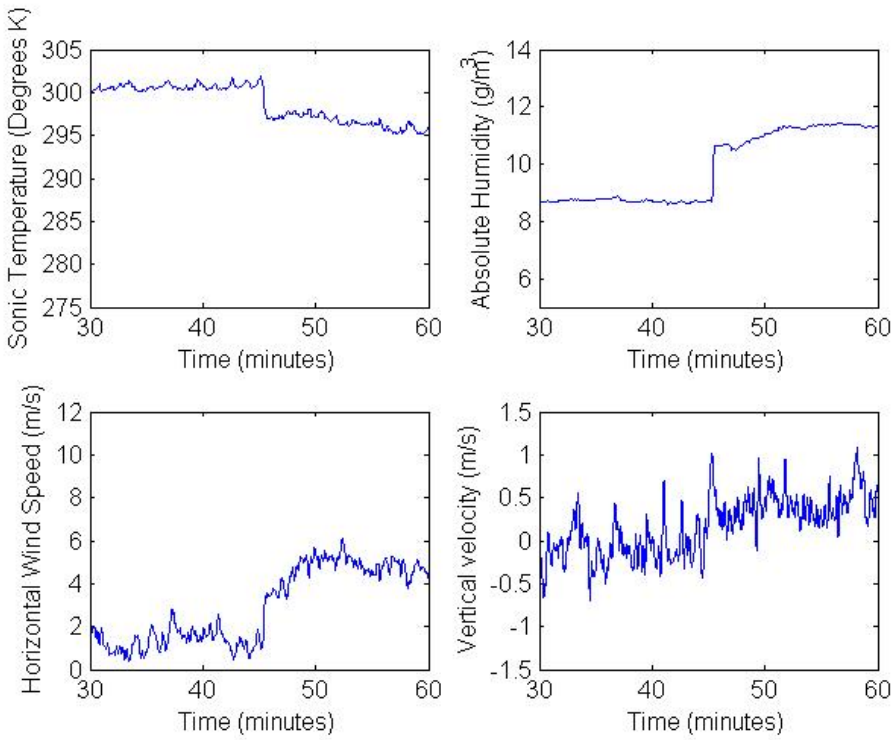

Figure 12. Wind humidity and temperate from 2130-2200 UTC

The time series of C_n^2 from the same period reveals two interesting features, Fig. 13. First, the optical C_n^2 values are actually lower than the RF C_n^2 values prior to the sea breeze. Second there is a massive spike in the RF C_n^2 values (~1.5 orders of magnitude) at the sea breeze front.

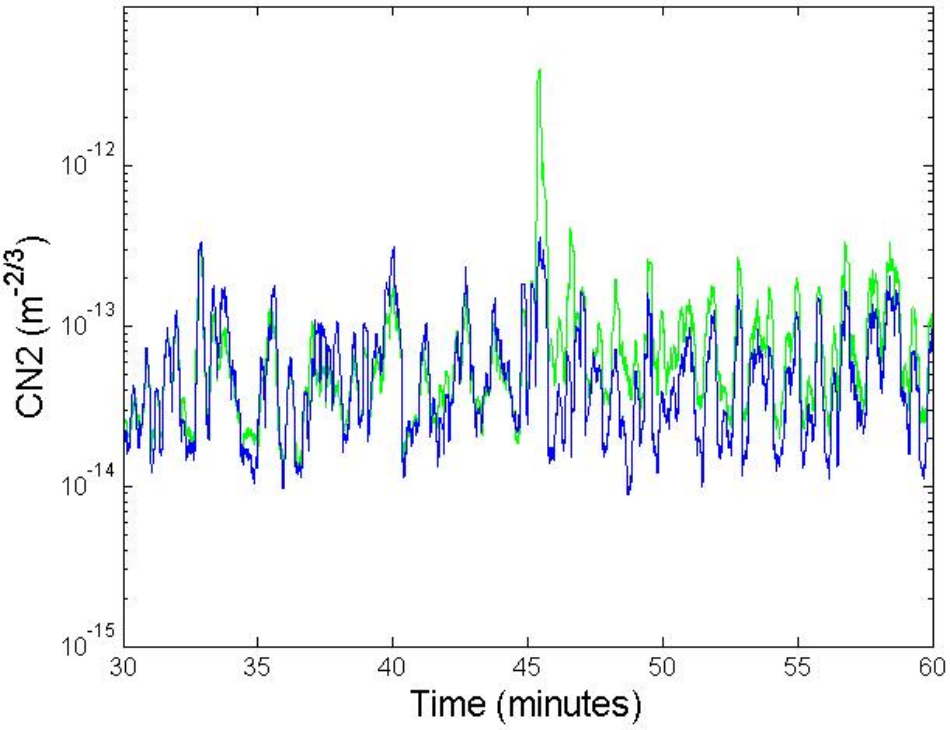

Figure 13. RF C_n^2 (green) and optical C_n^2 (red) from 2130-2200 UTC

Eqs. (5), (11) and (12) for C_n^2 show that the RF C_n^2 includes the optical C_n^2 (solely temperature dependant) plus terms that take into account moisture with the moisture term in the numerator and the temperature values in the denominator. To achieve RF C_n^2 values lower than the optical C_n^2, temperature and humidity values must be positively correlated and the changes in humidity small enough between sample points that the resulting change in RF C_n^2 is less than the change in optical C_n^2. If the temperature and humidity changes are negatively correlated the cross correlation term (term 3 in Eq. (7)) has a large value and produces RF C_n^2 refractivity fluctuations that are greater than seen for the optical case

Fig. 14 is a plot of the temperature humidity correlation during 30 minutes, 15 minutes before, during and 15 minutes after the sea breeze. Based on Kolmogorov theory the correlation coefficient will always be $\pm$ 1 (Hill 1989).

Because the correlation coefficients include an average of 30 seconds of data and the LI-7500 is ~10cm offset from the CSAT-3 paths, the correlation coefficients of exactly one are not shown. The overall change in the sign of the correlation coefficients is evident in the data.

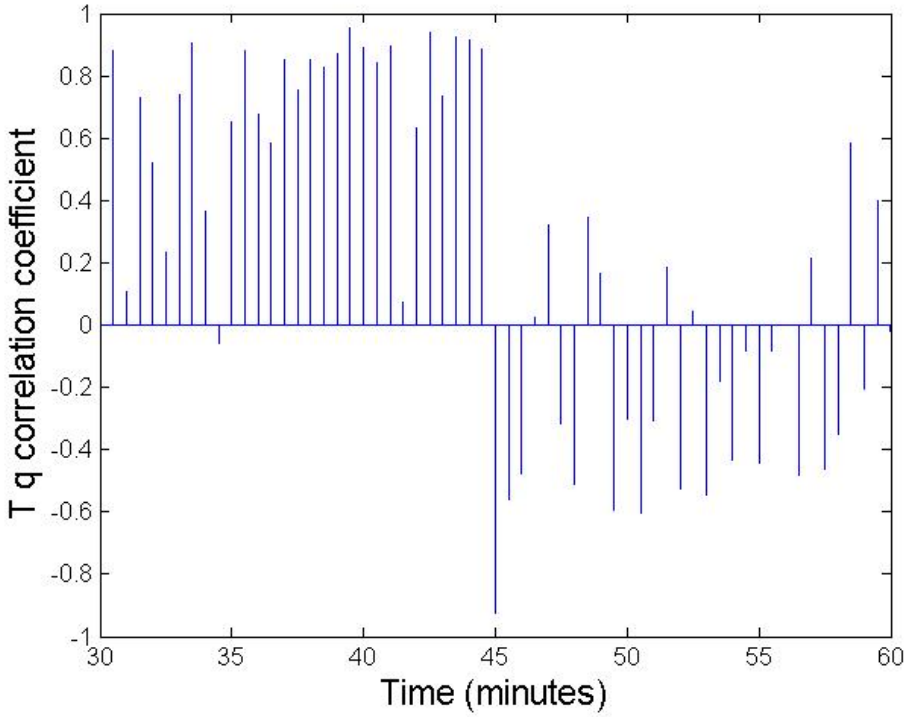

Figure 14. Temperature and humidity correlation coefficient from 2130-2200 UTC

3. Sea Breeze Boundary

The high frequency data allowed for a detailed examination of the frontal passage which lasted ~30 seconds. Within this 30-second period the power spectral density of N continued to follow the $f^{-5/3}$ dependence expected by Kolmogorov theory, Fig. 15. The temperature and humidity correction coefficients averaged for every second showed a distinct shift at 45.4 minutes, Fig. 16.

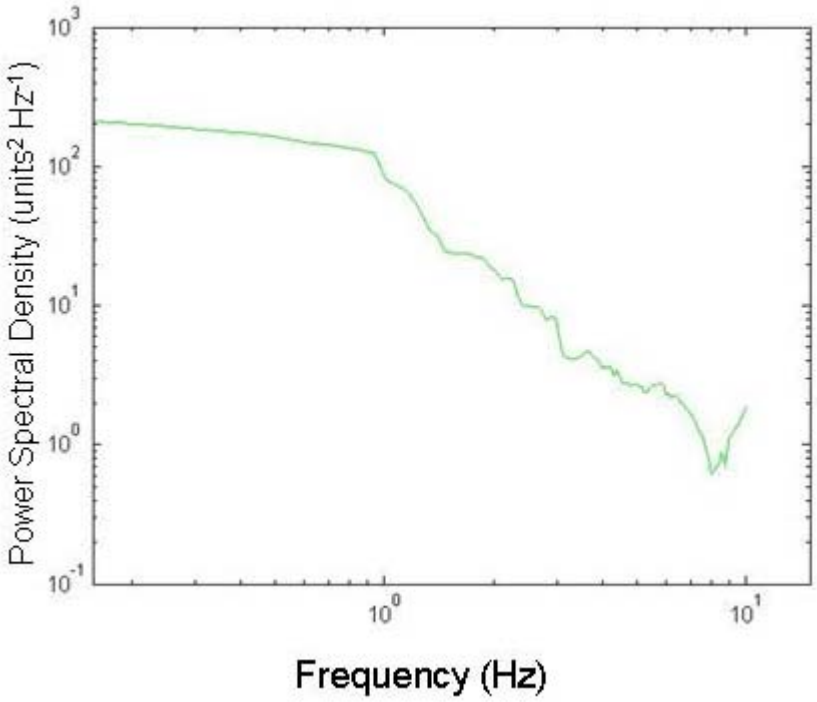

Figure 15. Power spectral density of N as sea breeze boundary passed, 30 seconds in the 2145Z minute

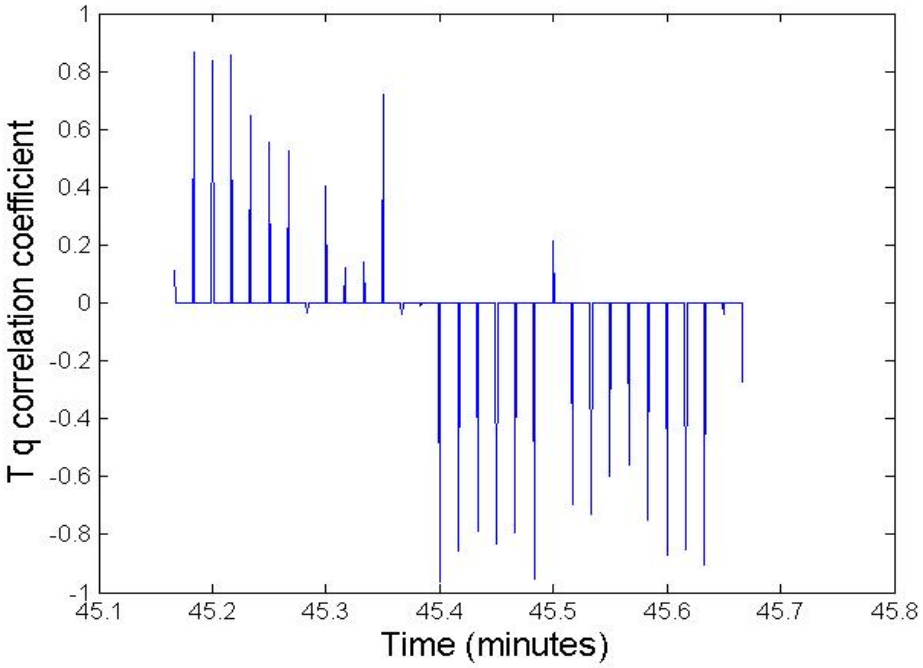

Figure 16. Temperature and humidity correlation plotted every second during boundary passage.

C. 23 FEBRUARY 2006

1. General Conditions

This day also had a sharp sea breeze front as seen in Fig. 17. There were weak synoptic forcing conditions with offshore winds less than 4 m s^{-1}. Clear skies as indicated by the shortwave irradiance curve permitted strong solar heating as indicated on the temperature plot. At approximately 2115 UTC (1315 PST) the passage of the sea breeze front was clearly marked by a rapid change in wind direction from offshore (~080^{o}) to onshore (~270^{o}) at the field site location and by velocity increasing (from ~2 m s^{-1} to above 6 m s^{-1}), and with increasing dew points and decreasing temperatures. As seen for 17 November 2005, the significant events that produced changes in C_n^2 were the wind speed increase that increased the mixing, and the airflow temperature and humidity changes causing different vertical gradients in the overlying airflow.

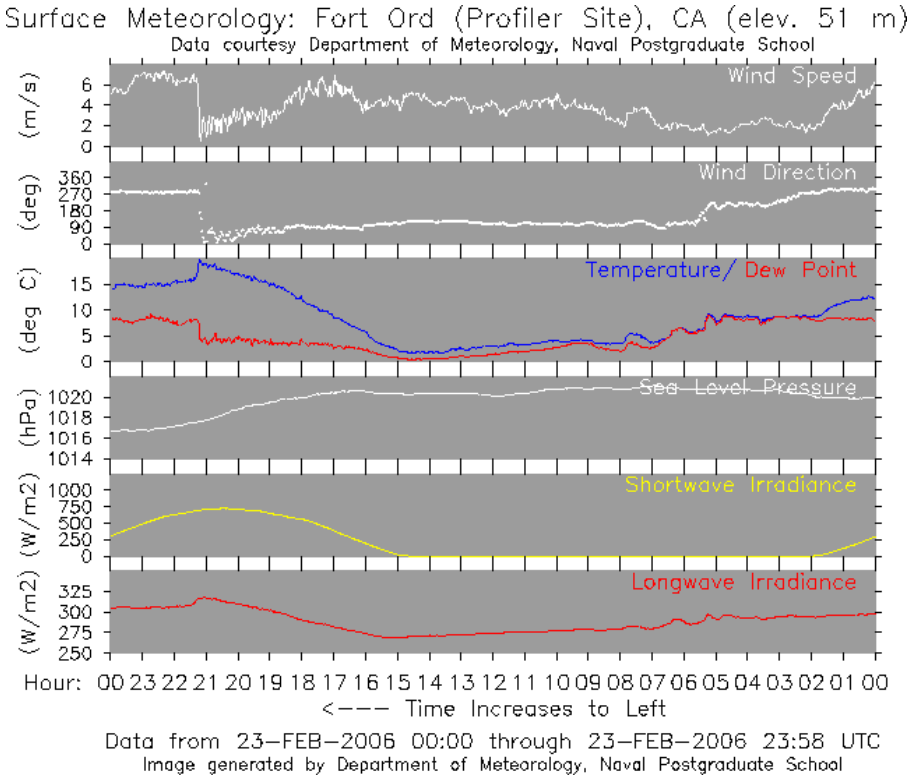

Figure 17. Weather summary for 23 February 2006

2. Sea Breeze Shift

The temperature shift is not as distinct and in the pervious case dropping ~4°K in ~7 minutes. The winds jump from a mean value near 2 m s^{-1} to a main value near 7 m s^{-1} in the same 7-minute period. The absolute humidity values to make the sharp jump noted the previous case going from 9 g m^{-3} to 12 g m^{-3} in ~30 seconds, Fig. 18.

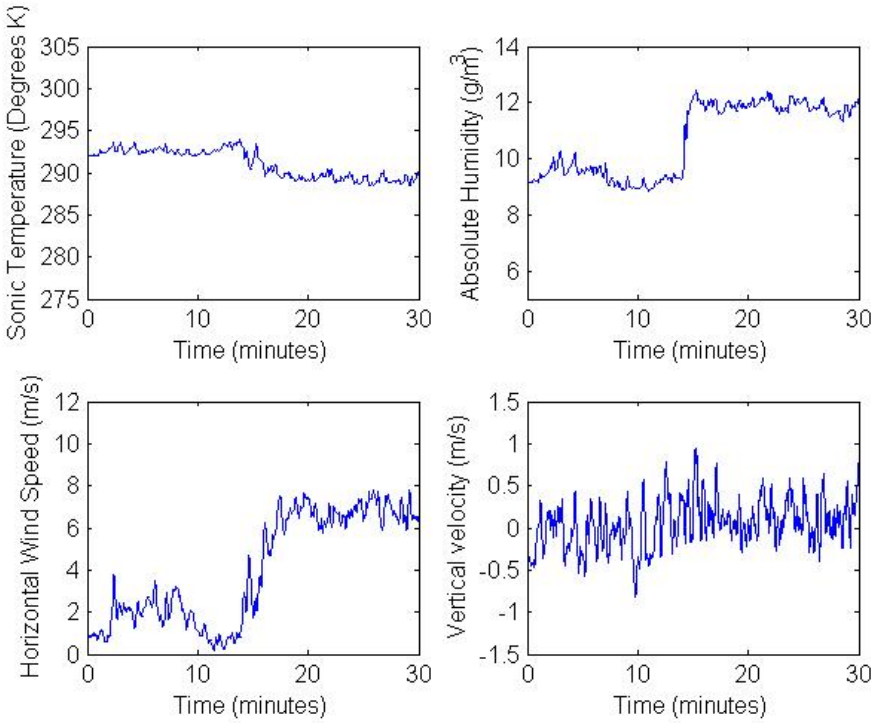

Figure 18. Wind humidity and temp 2100-2130 UTC

During this event the RF C_n^2 exceeded the optical C_n^2 before and after the sea breeze front passed, Fig. 19, with a noticeable spike (~1 order of magnitude) during the passage of the front. This also corresponds with a temporary reversal of the temperature humidity correlation coefficients during the passage, Fig. 20. Fig. 20 also shows that the correlation between temperature and humidity was mostly positive. Since Fig. 19 shows that the RF C_n^2 exceeded the optical, this implies that the humidity fluctuations had to exceed the temperature fluctuations throughout the entire period.

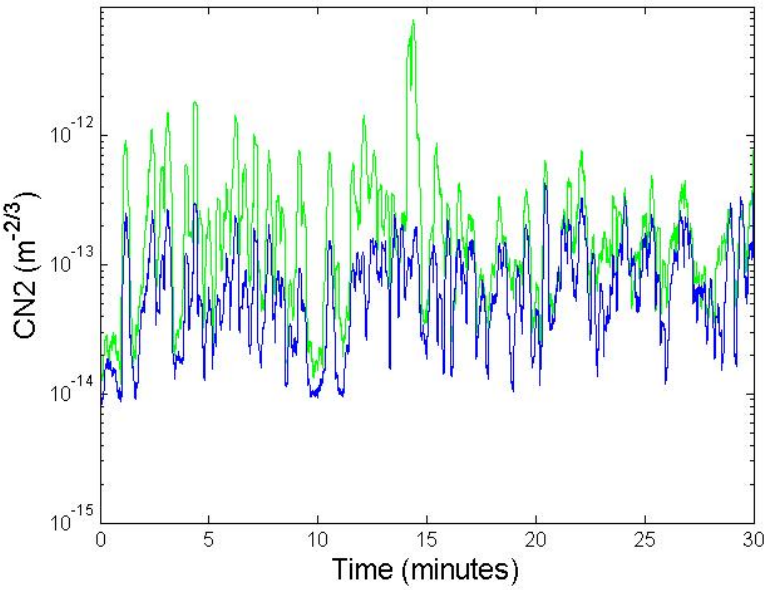

Figure 19. RF C_n^2 (green) and optical C_n^2 (blue) from 2100-2130 UTC

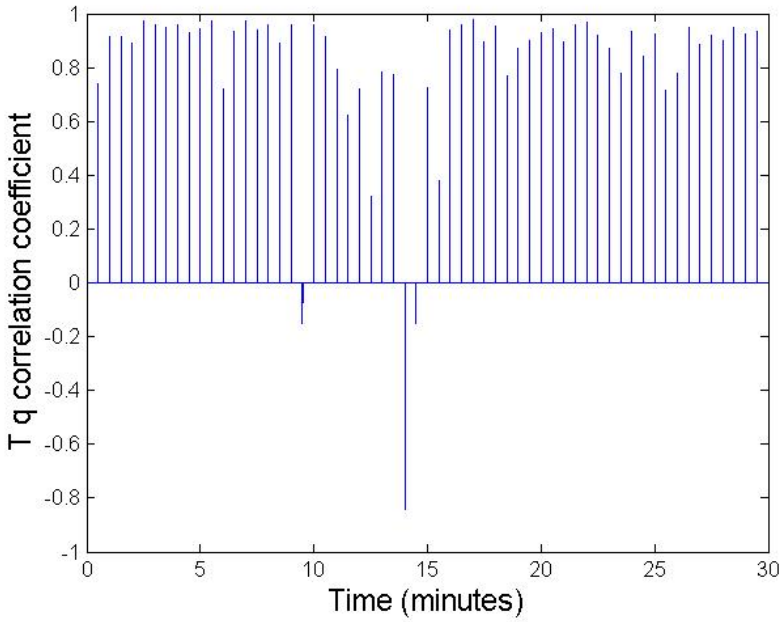

Figure 20. Temperature and humidity correlation coefficient from 2100-2130 UTC

D. 26 NOVEMBER 2005

1. General Conditions

This day had a stronger synoptic patter the resulted in westerly flow nearly all day. In the three hours prior to sunrise and the three hours after sunrise and easterly land set up for brief periods but was not able to maintain. The longwave irradiance plot indices some brief periods with clouds during the night, but skies were predominately clear during the period, Fig. 21.

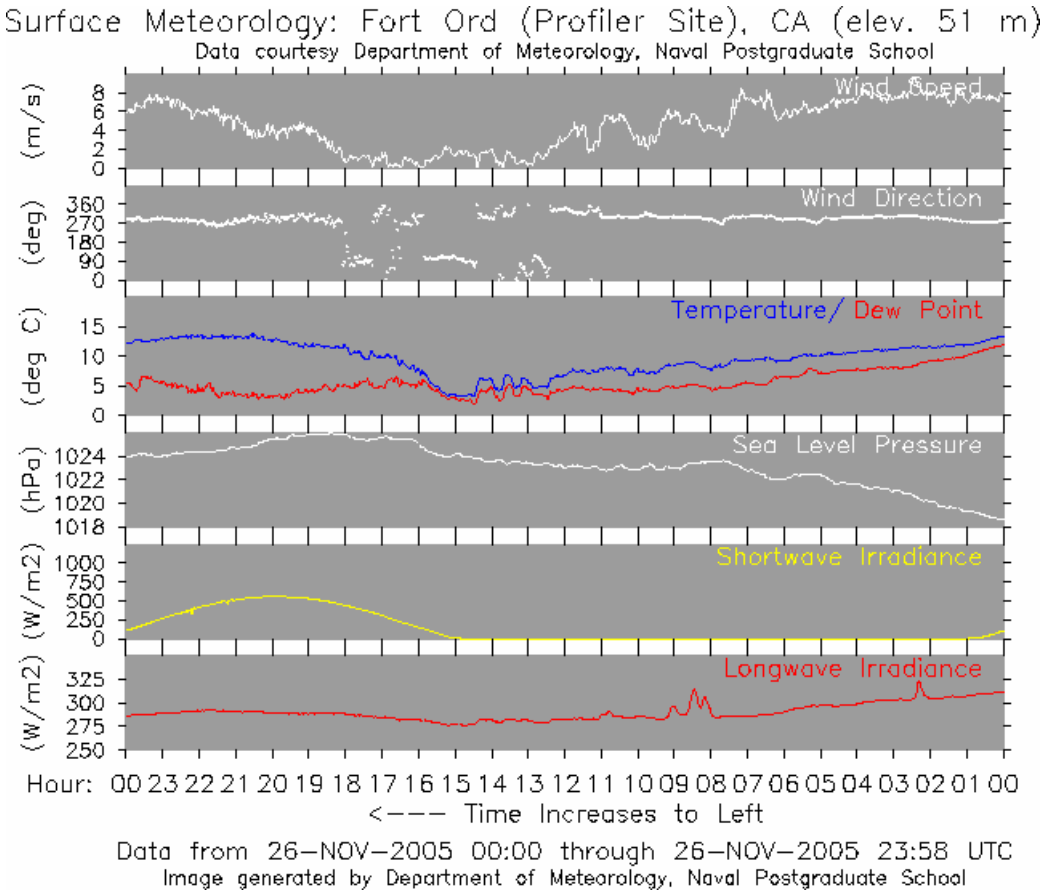

Figure 21. Weather summary for 26 November 2005

2. Cn^2 and Temperature-humidity Correlation

During the overnight hours, the RF C_n^2 exceeded the optical C_n^2 by nearly one order of magnitude, Fig. 22, while the temperature and humidity correlation coefficients remained primarily negative, Fig. 23. In the three hours prior to sunrise, when the land breeze intermittently set up, correlations varied between positive and negative as the optical and RF C_n^2 had similar magnitudes. After sunrise (~1600-1800 UTC) the winds remained light (< 2 m s^{-1}) and convection dominated the mixing processes. During that period RF C_n^2 increased by nearly 2 orders of magnitude when the temperature and humidity were negatively correlated.

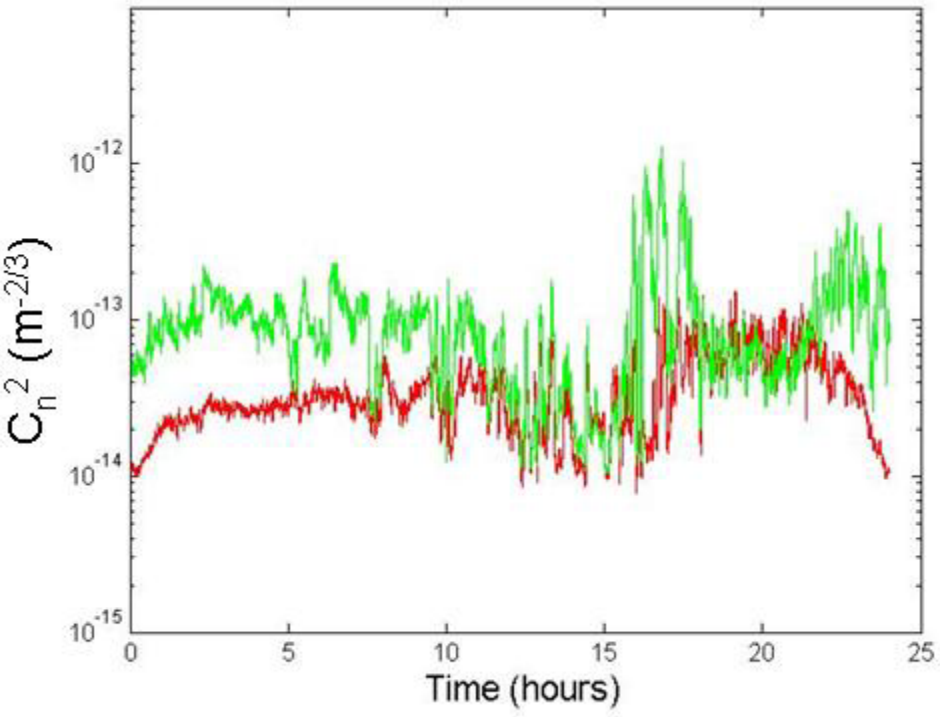

Figure 22. 24-hour plot of C_n^2, red: optical, green: RF

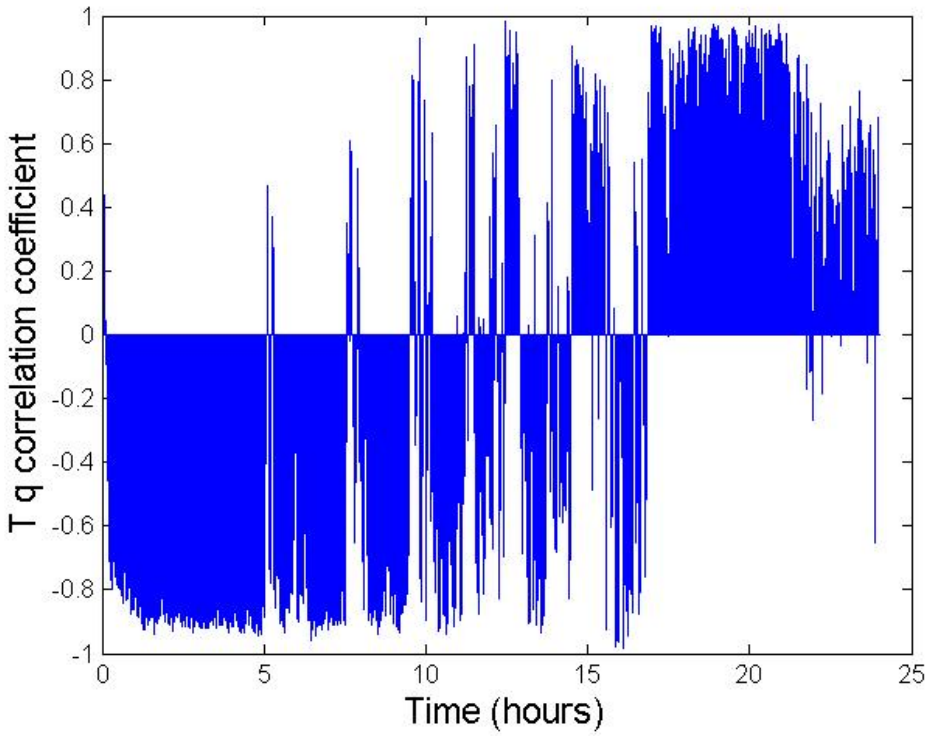

Figure 23. 24-hour plot of temperature and humidity correlations (90 sec averages)

IV. CONCLUSIONS AND RECCOMENDATIONS

A. DATA AND EQUIPMENT

This thesis studied the interaction of the atmospheric temperature and moisture fluctuations and their effects on the optical (dry) and RF (moist) refractive index structure function parameter, C_n^2, using data obtained with a turbulence instrumentation suite at the NPS Marina Field Site, Marina Airport, Marina, CA. The instrumentation consisted of a sonic anemometer, fine wire thermocouple and open path gas water vapor analyzer sampled at 20 Hz., The equipment and sampling approach were suitable for determining values of C_n^2 directly from the structure function for both the dry and moist indices of refraction. The onset of the sea breeze produced a strong increase of one to two orders of magnitude in the RF refractive fluctuations, when the cross correlation between temperature and humidity changed signs.

B. RECOMMENDATIONS FOR FUTURE STUDY

This study, although limited in scope, indicates that further data processing could reveal the relationships between the underlying atmospheric conditions that produce the optical and RF refractivity fluctuations Since the correlation of temperature and humidity values play a significant role in enhancing the RF C_n^2, a more extensive study could allow one to predict the sign of the correlation coefficient in advance. Identifying a larger number of days with data sets uninterrupted by dropouts or equipment failure, would allow the processing of more days. This could reveal additional diurnal and seasonal patterns in the data as well as the creation of meaningful averages. Data collected at other locations such as the East coast of the US would be beneficial since the inversion conditions and moisture concentrations are appreciably different than for the Pacific Coast.

THIS PAGE INTENTIONALLY LEFT BLANK

LIST OF REFERENCES

Arya, S.P., 2001: *Introduction to Micrometeorology.* Academic Press, 414 pp.

Beland, R. R., 1996. *Propagation through atmospheric optical turbulence*. Vol. 2, *The infrared & electro-optical systems handbook*, SPIE Optical Engineering Press, 383 pp.

Campbell Scientific, cited 2007: CSAT-3 instruction manual. [available online at http://www.campbellsci.com/documents/manuals/csat3.pdf]._____, cited 2007: Fine Wire brochure. [Available online at http://www.campbellsci.com/documents/lit/b_fw05-fw3.pdf].

Eaton, F.D., 2005: Recent developments of optical turbulence measurement techniques. *Proceedings of SPIE* , Vol. 5793, doi:10.1117/12.604904.

Fort Ord Terminal Forecast Reference Notebook, 1977. Acquired from Air Force Combat Climatology Center webpage: https://notus2.afccc.af.mil/SCISPublic/.

Hill, R.J., 1989: Implications of Monin-Obukhov Similarity theory for scalar quantities. *Journal of the Atmospheric Sciences,* **46,** 2236-2244.Li-Cor, cited 2007: LI-7500 description. [available online at http://www.licor.com/env/Products/GasAnalyzers/7500/7500_description.jsp].

Lim, S.S.M., 2003: Investigation of outer length scale in optical turbulence. M.S. thesis, Physics Department, Naval Postgraduate School, 53 pp.

Max, C. E., cited 2007. Lecture 3: Diffraction and Atmospheric Turbulence. [Aviable online at http://www.ucolick.org/~max/289C/Lectures/Lecture3/Lecture3.v1.sm_output.pdf] .

Parker, S., 2002: Atmospheric optical turbulence comparisons: MM5 and COAMPS. M.S. thesis, Physics Department, Naval Postgraduate School, 87 pp.

Roper, D.S., 1992: Investigation of systematic effects in atmospheric microthermal probe data. M.S. thesis, Physics Department, Naval Postgraduate School, 98 pp.

Rueger, J.M., cited 2007: Refractive Index Formulae for Radio Waves. [Available online at http://geodesia.ufsc.br/Geodesia-online/arquivo/FIG/2002%20Washington/Js28/JS28_rueger.pdf].

Stankov, B.B., E.E. Gossard, B.L. Weber, 2003: Humidity gradient profiles from wind profiling radars using the NOAA/ETL advanced signal processing system (SPS), *J. Atmos. Oceanic Technol.*, **20**, 3-22.

Tatarski, V. I., 1961: *Wave propagation in a turbulent medium*. McGraw-Hill, 285 pp.

Walters, D.L., and K.E. Kunkel, 1981: Atmospheric modulation transfer function of desert and mountain locations: the atmospheric effects on r_o, *J. Opt. Soc. Am.*, **71**, 397-405.

INITIAL DISTRIBUTION LIST

1. Defense Technical Information Center
   Ft. Belvoir, Virginia

2. Dudley Knox Library
   Naval Postgraduate School
   Monterey, California

3. Air Force Weather Technical Library (AFWTL)
   Asheville, North Carolina